TUTORIAL REVIEW

Check for updates

Approaches for selectivity improvement of conductometric gas sensors: an overview

Jing Li, Hongchao Zhao, Yanjie Wang and Yong Zhou [iD] *

Conductometric gas sensors (CGS) have been extensively explored in recent decades owing to easy fabrication and miniaturization, low cost and distributable detectability. Among numerous performance parameters, selectivity is a critical one to evaluate the operation quality of CGS in diverse application scenarios such as environment monitoring, food quality assessment, individual healthcare, *etc*. Nevertheless, in most preceding work either the underlying mechanism for the shown selectivity is not explained clearly or the strategies to improve the selectivity are not detailed, which necessitates an urgent need to address these. Also, there is still a lack of comprehensive summaries reported in this aspect thus far. A favorable selectivity always means a stronger sensitivity toward a specific gas than that toward other interference gases. Thus, it is very essential to conduct a comprehensive overview to understand the sensitivity, selectivity and their relationships from both quantitative and qualitative perspectives. In this review, the sensing mechanism of CGS is first studied according to the selectivity coefficient simultaneously concluding the factors that influence the detection selectivity. Subsequently, chemical and physical modification strategies to improve the selectivity are discussed. Finally, challenges and perspectives of the selectivity optimization methods are proposed for future research.

1. Introduction

The global sensor market has witnessed an ever-increasing expansion. Among diverse sensor species, gas sensors are extensively applied in numerous scenarios such as explosive or toxic environments, Internet of Things (IOT), indoor air quality monitoring,[1] medical diagnostics,[2] food quality assessment,[3] *etc.* Its market is expected to reach 2.28 billion $ dollars by 2025. When surface-active nanomaterials come into contact with gas, the gas–solid interactions will change their inherent physicochemical parameters such as conductivity, capacitance, work function, optical properties, and reaction energy due to the large surface area, abundant functional groups, flexible adjustability of the structure–property relation, and environmental susceptibility.[4–8] We roughly summarize approximately 900 research papers over the past decade with the search keywords "nanomaterials" and "gas sensing" *via* Web of Science as shown in Fig. 1. The results indicate that conductive gas sensors (CGS) with the merits of low cost, easy manufacturing and signal processing, and high sensitivity have gained the most popularity. However, in order to improve the cost-effectiveness of CGS in practical applications, further optimization and improvement are still needed in terms of sensitivity, selectivity, response/recovery time, operating temperature, *etc.*

Of different performance parameters, selectivity is one of the most crucial indicators for evaluating the quality of CGS. Gas sensors with ideal selectivity can readily ascertain the detailed species and concentration of a specific gaseous component without any interference from other coexisting ones, which ensures an accurate and reliable gas detection. However, selectivity is often overlooked in most preceding efforts. Therefore, it is urgently essential to offer potential methods as theoretical basis for instructing the improvement process. Recently, the methods that leverage special catalytic components such as precious metals or rare earth metal oxides, filters, and sensor arrays, and the latest research
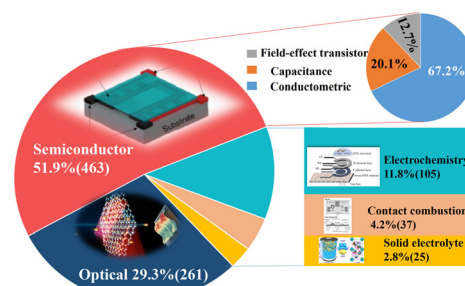
Key Laboratory of Optoelectronic Technology and System of Ministry of Education, College of Optoelectronic Engineering, Chongqing University, Chongqing 400044, People's Republic of China. E-mail: zhyf@cqu.edu.cn

Fig. 1 Summary of academic papers published on nanomaterial based gas sensors in the past decade.

using binary metal oxides[9] and hierarchical metal oxides[10] have emerged to boost the sensitivity and selectivity. Meanwhile, a few review articles in recent years had reported the modification of the selectivity of gas sensors.[9–17] For example, G. Korotcenkov et al.[9] discussed the engineering methods for improving the selectivity of CGS. Alternatively, M. Wusiman et al.[14] provided chemical modification methods, but did not systematically elaborate the selectivity enhancement from the basic properties of gas molecules such as mass, charge, etc. In another report, H. Hashtroudi et al.[13] studied the hybridization effect of two-dimensional (2D) materials on sensor selectivity and sensitivity as well as the sensing mechanism. As claimed by the authors, the hybridization offered more surface sites and then enhanced the collective performance. However, this research was only limited to 2D hybrid materials operated at room temperature. Another group[18] detailed the factors that affected the selectivity of gas sensors as well as the techniques to improve the selectivity but from both spectral and nonspectral aspects.

According to the current endeavors mentioned above, this review comprehensively discusses the latest progress in improving the selectivity of CGS through both chemical and physical methods. The basic principles for each method are introduced from the perspectives of electron sensitization, chemical sensitization, and affinity modulation between target molecules and sensing materials. Also, the problems encountered are emphasized. Finally, an overall perspective on the issue of selectivity, as well as the challenges and prospects, is presented, with the aim of paving the way for optimizing future gas sensors with excellent selectivity.

2. Strategies to improve the detection selectivity

The fluctuation of the gaseous composition and concentration within the test environment would change the electronic properties of the sensing material for CGS. Recently, researchers have explained these phenomena from many perspectives, such as the electronic core–shell structure including the electron depletion layer (EDL) and hole accumulation layer (HAL),[19,20] bulk resistance-control model,[21] and gas-diffusion mechanism.[22] However, the sensing mechanism of CGS is generally explained by gas–solid interactions such as ion oxygen adsorption and direct charge transfer, which is also well known as the receptor function of sensitive materials (as shown in Fig. 2). CGS mainly employ metal oxide semiconductors (MOS) and 2D layered nanomaterials including carbon nanomaterials (e.g., graphene and its derivatives), transition metal dichalcogenides (TMDs), MXene, black phosphorus (BP), etc., as the sensing materials. Although electron exchange occurs between gas molecules and sensitive materials in both cases, the sensing pathways are absolutely different. MOS predominantly follow the surface-oxygen adsorption model,[23] wherein gas molecules directly react with these active oxygen species. However, 2D nanomaterials are more suitable for the charge transfer model with less
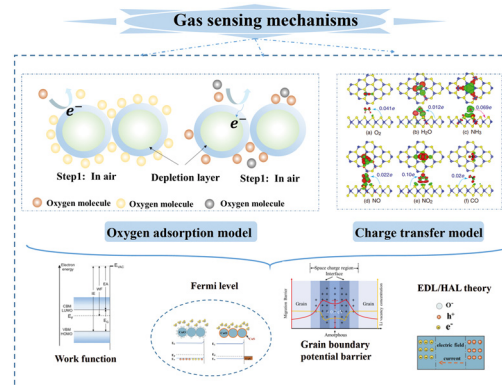

Fig. 2 Gas sensing mechanisms of CGS: classification and summary.

dependence on surface oxygen species,[24] which involves direct electron exchange between sensitive materials and gas molecules.

However, the vast majority of CGS undergo electron exchange between their surfaces and gas molecules regardless of the gas species, which leads to the inherent weak selectivity. It is well known that selectivity indicates the ability to distinguish a specific gas from others. It could be quantitatively expressed by the ratio of the sensor signal toward the target gas (S_{gas}) to that toward the interfering one ($S_{interferent}$), which was also termed as the selectivity coefficient. So the sensor selectivity could be improved by augmenting the target response and/or suppressing the interfering signal (Fig. 3). According to the sensing mechanism, the receptor function of CGS involves the ability of the material surface to interact with the target gas, which is determined by the adsorption and reaction processes. Therefore, the receptor function is closely related to the adsorption affinity, catalytic ability, and surface acidity/alkalinity of the sensing material as well as the reactivity of gas molecules. The enhancement of receptor function depends on the type and microstructure of the sensing material, which can be achieved through chemical methods such as doping, composite construction, and surface modification. In addition, the same target could be reached by reducing interference
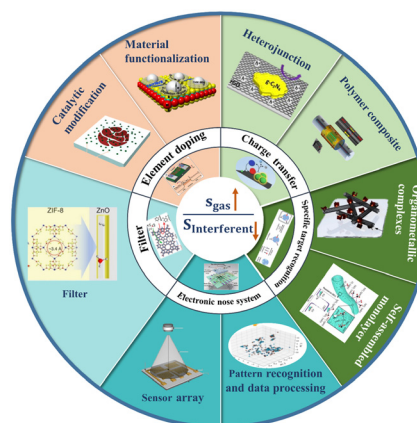

Fig. 3 The strategies to improve the sensor selectivity.

Table 1 Summary of element-doped gas sensors

Material type	Material	Dopant	Gas/Conc. (ppm)	Response[a]	Selectivity coefficient	Ref.
Metal doping	SnO_2	Pd	o-Xylene/5	17	HCHO, benzene, H_2 (<7)	25
	SnO_2	Pd–Au	Acetone/20	50	CH_3COCH_3, C_2H_5OH, HCHO (<4)	26
	SnO_2	Pd	H_2/1000	45.7	—	27
	ZnO	Pt–Au	H_2/1%	1.58	O_2, NO_2, CO, CO_2, N_2 (<1.04)	170
	ZnO–rGO	Ag	C_2H_2/100	21	H_2, O_2, NO_2, CO, CO_2 (<3)	29
	NiO	Cr	o-Xylene/5	11	Toluene, benzene, ethanol et al. (<3)	30
Noble metal doping	rGO	Pd	H_2/1000	1.07	O_2, NO_2, CO, CO_2, N_2 (<1.01)	31
	rGO	Ag	NH_3/10	10	NH_3 (>15)	32
	rGO	Ag	NO_2/50	1.74	CH_3OH, C_2H_5OH, C_7H_3, RH (<1.3)	33
	MoS_2	Au	Acetone/10	10	Acetaldehyde, ethanol, toluene (<15)	34
	MoS_2	Pd	NH_3/100	10	NH_3 (<4), NO_2 (<1)	35
	WS_2	Ag	NO_2/500	7.67	—	171
	WS_2	Pt	NH_3/250	10	—	172
	BP	Pt	H_2/500	500	Acetone, ethanol, toluene (<15)	36

Conc.: concentration. ^{a} Response $= \dfrac{R_g}{R_o}$.

signals through filter membranes as well as utilizing gas sensor arrays and temperature/humidity regulation.

2.1 Element doping

As a common means of catalysis sensitization, element doping could optimize the sensing performance. According to the types and working principles of dopants, they can be divided into common metal doping (no noble metal), precious metal doping, and bimetallic doping. Common metal doping mainly improves the electron exchange rate by changing the band structure of the parent material, and focuses on chemical sensitization. Noble metal doping (Pd, Pt, Au, etc.) could lead to not only electron sensitization by changing the crystal structure, the content of oxygen vacancies and adsorption sites, and the reaction rate, but also chemical sensitization by dissociating the adsorbed gas molecules more easily. In addition, bimetallic doping was verified feasible to deliver better selectivity. Table 1 summarizes some related cases through element doping.[25–36]

2.1.1 Common metal doping. Common metal doping mainly achieves chemical sensitization through catalytic action. Currently, the catalytic effect includes the direct catalysis reaction and target molecule dissociation. In addition to promoting the oxidation of the target gas itself during the sensing process, the catalyst also accelerated the mutual reaction between the target gas and oxygen species within the sensing material. H. J. Kim et al.[30] employed layered Cr-doped NiO nanostructures for selective and sensitive detection of xylene, ethanol, formaldehyde and toluene (Fig. 4a). Obviously, low-concentration doping of Cr element effectively facilitated the oxidation of methyl benzene at high temperature into more active benzyl alcohol or benzaldehyde, ultimately improving the sensitivity and selectivity (Fig. 4b). The pure NiO sensor did not show any selectivity while the 1.15Cr-NiO one was much more responsive to o-xylene (11.61) and toluene (7.81) than to benzene (1.42), ethanol (2.59), formaldehyde (2.03), H_2 (1.44)

and CO (1.31). In addition, the response and baseline resistance were remarkably increased after introducing 1.15–2.56% Cr.

The catalyst could also dissociate the target gas molecules into gaseous intermediates with higher polarity and reactivity and thus favor a faster reaction. For instance, Y. J. Hong et al.[25] demonstrated a continuous, single-step and large-scale preparation of Pd-supported SnO_2 yolk–shell balls. These nanostructures exhibited high response to methyl groups (e.g., toluene) and a very low one to various interfering gases such as xylene and benzene, rendering them suitable for accurate indoor air-quality monitoring (Fig. 5). Within Pd-loaded SnO_2 hollow microreactors, toluene was dissociated into smaller species with different chemical properties, resulting in more complex gas–solid reactions. As benzene was more stable than xylene and toluene, its difficult dissociation led to a low response. The weak reaction to ethanol, formaldehyde, and H_2 could be explained by the complete oxidation of these gases to less reactive ones.
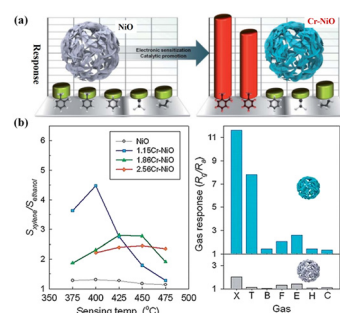
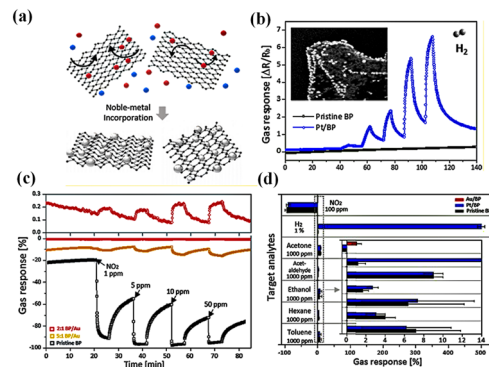

Fig. 4 (a) Cr-doped NiO hierarchical nanostructure based methyl benzene sensors. (b) The ratio of the response toward 5 ppm o-xylene to that toward 5 ppm ethanol ($S_{xylene}/S_{ethanol}$) of NiO based sensors with temperature as well as the sensor response toward 5 ppm o-xylene (X), toluene (T), benzene (B), formaldehyde (F), ethanol (E), hydrogen (H) and carbon monoxide (C) at 400 °C of pure NiO and 1.15Cr-NiO sensors. Reprinted with permission from ref. 30 copyright 2013, The Royal Society of Chemistry.
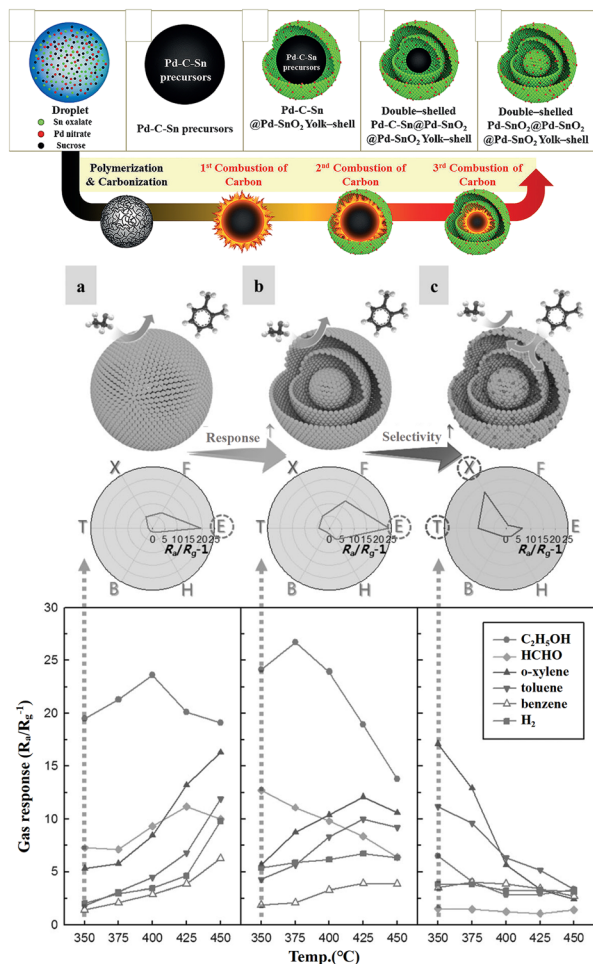
Fig. 5 Gas response of (a) dense SnO$_2$ spheres, (b) SnO$_2$ yolk–shell spheres and (c) Pd-loaded SnO$_2$ yolk–shell spheres toward various gases with temperature (B: benzene, H: H$_2$, E: C$_2$H$_5$OH, F: HCHO, X: o-xylene, T: toluene). Reprinted with permission from ref. 25 copyright 2014, The Royal Society of Chemistry.


Fig. 6 (a) Schematic illustration of Au- or Pt-modified few-layer BP, (b) gas response of pristine and modified BP sensors as function of H$_2$ concentration, (c) tunable response behavior of Au/BP sensors by controlling the Au content, and (d) response of all sensors to various analytes. Reprinted with permission from ref. 36 copyright 2017, American Chemical Society.

2.1.2 Noble metal doping. It was reported that noble metal doping was also conducive to selective gas detection with high response.[37] In addition to the catalysis effect, the hybridization effect of noble metals (Au, Ag, Pd, Pt, etc.) on the core sensing material could lead to electronic modulation such as p- or n-type doping for the performance adjustment. For example, pristine and Au nanoparticle (NP)-decorated MoS$_2$ separately exhibited p- and n-type behavior toward different volatile organic compounds (VOCs).[38] Here, the incorporation of Au NPs strengthened the interaction between NH$_3$ molecules and MoS$_2$ flakes.[39] This is the same case for Pd NP decorated MoS$_2$ nanoflakes toward H$_2$ sensing.[40] In another study,[36] the hybridization effect of Au or Pt on the sensing performance of BP was investigated in detail (Fig. 6a). Bare BP only detected paramagnetic molecules such as NO$_2$ and NO. When decorating BP with Pt or Au, a higher response toward H$_2$ and a lower one toward NO$_2$ with respect to pristine BP could be achieved (Fig. 6b and c). Compared with the previous efforts about H$_2$

sensing, the reported sensor here was the most sensitive (Fig. 6d).

Different noble metals possess inconsistent oxidation activities towards a specific gas. Based on this, the selectivity to different target gases could be improved by doping different noble metals. C. R. Jung et al.[41] prepared a CuO–CeO$_2$ composite doped with precious metals (Pt, Pd, and Ru) and evaluated its selective oxidation of CO in hydrogen-rich gas streams. The results indicated that Pt doping shows the highest oxidation activity for CO while Pd or Ru doping for H$_2$. This is because the doping behavior upshifts the binding energy of Cu within CuO–CeO$_2$ and suppresses the degree of copper phase separation. In addition, the type and loading capacity of precious metals will determine the degree of movement and separation, which leads to varying oxidation activities towards different gases. By adopting a suitable precious metal, the selectivity could be improved by increasing the target response.

2.1.3 Bimetallic doping. Single metal doping always exhibits some drawbacks such as easy agglomeration and uncontrollability. In recent years, bimetallic doping has been found to be capable of avoiding these unwanted features.[42–44] In addition, compared to single metal doping, bimetallic doping probably exhibits synergistic effects due to geometric effects, electronic interactions, and chemical reactions, which can simultaneously catalyze and sensitize the parent material, and thus improve the selectivity. For instance, K. Jiang et al.[42] reported Pd/Pt bimetallic-NP-doped In$_2$O$_3$ hollow microspheres that were synthesized using solvothermal and in situ reduction methods for H$_2$S detection. It was found that 1 at% Pd/Pt In$_2$O$_3$ composites exhibit strong selectivity and sensing performance (as shown in Fig. 7a and b). Fig. 7c shows the underlying sensing mechanism, wherein Pt NPs primarily enhance the gas sensitivity through chemical sensitization to promote the formation of chemically adsorbed oxygen. Then, a large amount of these oxygen species spill onto the surface of the
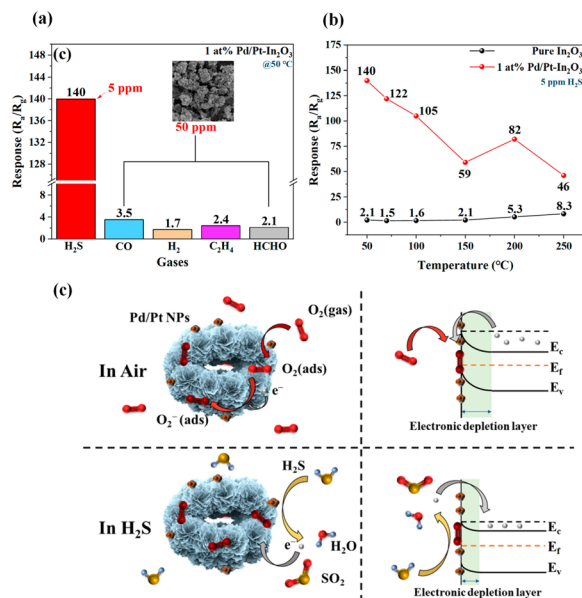
Fig. 7 (a) Response of 1 at% Pd/Pt-In$_2$O$_3$ to various gases (CO, H$_2$, C$_2$H$_4$, and HCHO). (b) Response of pure In$_2$O$_3$ and 1 at% Pd/Pt-In$_2$O$_3$ to 5 ppm H$_2$S at different temperatures. (c) Demonstration of the gas-sensing mechanism of 1 at% Pd/Pt-In$_2$O$_3$, the left side is a simulation diagram of the microsphere, and the right side is an energy-band diagram. Reprinted with permission from ref. 42 copyright 2023, MOPI.

parent material, thereby improving the sensitivity. Meanwhile, Pd NPs boost the selectivity through electron sensitization. Due to the higher work function of Pd NPs (5.5 eV) compared to In$_2$O$_3$ (5.0 eV), a Schottky barrier is formed between Pd NPs and In$_2$O$_3$. With respect to either single-metal catalysts, Pd/Pt bimetallic NPs can further enhance their catalytic activity due to the synergistic effect. In addition, water molecules are generated during the reaction between H$_2$S and chemically adsorbed oxygen, which then react with Pd to form Pd(OH)$_2$ with low catalytic activity, and

reduce the activity of Pd.[45] However, doping an appropriate amount of Pt can weaken this influence.

Generally, element doping can introduce impurity levels within the band gap of the parent material. These impurity levels could act as recombination centres for electrons and holes. Also, doping semiconductors with a wide band gap may induce some undesirable properties or behaviors. This is detrimental to the sensor performance. In addition, the control of the doping ratio needs to be studied as more doping will cause severe agglomeration while less doping cannot achieve the desired effect.

2.2 Composite construction

To achieve a better selectivity, composite construction is another feasible method as it can suppress the problems of unwanted impurity levels and agglomeration encountered through element doping while achieving an improved performance compared with a single material. An interfacial depletion layer is always produced, accompanied with specific electron transfer, conformational changes, *etc.*, which eventually promotes the selectivity. Thus, the resistance change during the sensing process is amplified for a stronger selectivity, as summarized in Table 2.[46–62] In addition, the unique electron transfer, conformational changes, and target molecule-matched cavities probably enable a highly selective response for polymer-based composites, as concluded in Table 3.[63–70]

2.2.1 Heterojunction nanostructures. Heterojunction nanostructures were developed to address the selectivity limitations always faced by single materials.[71] There are three types of heterojunctions between two different semiconducting materials, namely, p–p, n–n, and p–n ones. Heterojunctions mainly improve the selectivity by amplifying the modulation effect of carrier density. Table 2 summarizes the related research on heterojunction-based gas sensors.

Table 2 Heterojunction-based gas-sensing performance[46–62]

Material type	Materials	Gas/Conc. (ppm)	Response	Selectivity coefficient	Ref.
Metal oxide	ZnO–CuO	H$_2$S /100	25	NH$_3$, EtOH, butanol, acetone ($<$2)	46
	Cu$_2$O–SnO$_2$	H$_2$S /50	1.45	NH$_3$, NO, H$_2$, toluene ($<$1.2)	47
	In$_2$O$_3$–SnO$_2$–Al$_2$O$_3$	NO$_2$/450	632	CO$_2$ ($<$10)	48
	Fe$_2$O$_3$–In$_2$O$_3$	NO$_2$/5	5.4	CO ($<$1.25)	49
	SnO$_2$–NiO	Ethanol/1000	576	Methanol, ammonia, acetone ($<$100)	50
	Al2O$_3$–TiO$_2$	Ethanol/1000	1108	H$_2$S, CH$_3$OH ($>$350)	51
	SnO$_2$–TiO$_2$	Acetone/100	14	HCHO, CH$_3$OH,C$_2$H$_5$OH,NH$_3$ ($<$7)	52
	ZnO–TiO$_2$	Acetone/100	23	CO, C$_2$H$_5$OH ($<$7)	53
	SnO$_2$–ZnO	Methanol/50	18	Ammonia, benzene, acetone ($<$8)	54
Low-dimensional materials	rGO–carbon nanodot	NO$_2$/25	2.2	DMMP, ethanol, methanol ($<$1.02)	55
	g-C$_3$N$_4$–rGO	NO$_2$/1	1.8	NH$_3$, SO$_2$, toluene, hexane ($<$1.1)	56
	WS$_2$–CuO	H$_2$S /0.5	37	SO$_2$, NO$_2$, NH$_3$, CO, CO$_2$ ($<$2)	57
	BP^a–SnO$_2$	H$_2$S /5	8.1	CO$_2$,HCHO, H$_2$S, C$_3$H$_8$O ($<$3)	58
	BP^a–ZnFe$_2$O$_4$	Acetone /0.1	4.9	SO$_2$, NH$_3$, NO, CO, CO$_2$, H$_2$S ($<$3)	59
	ZnFe$_2$O$_4$ZnSnO$_3$	Acetone /30	63.3	Ammonia, benzene, toluene ($<$20)	60
	rGO/WS$_2$	NH$_3$/10	2.78	Acetone, ethanol, methanol ($<$1.2)	61
	MXene/SnO$_2$	NH$_3$/50	1.4	Formaldehyde, ethanol ($<$1.04)	62

CED: cyclic electrochemical deposition; CVD: chemical vapor deposition.

Table 3 Summary polymer-based composite materials and their sensing performance

| Polymer type	Materials	Gas/Conc. (ppm)	Response	Selectivity coefficient	Ref.
CPs	PANI/MWCNTs	$NO_2/100$	1.28	NH_3 (<1.03)	63
	PEDOT:PSS/cellulose nanofibers	$NH_3/1$	1.05	SO_2, CO, H_2S, acetone (<1.02)	64
	P3HT	$NO_2/1$	50	SO_2, CO, H_2S, NH_3 (<3)	65
	n-Eicosane and carbon powder	Toluene/25	1.18	Benzene, chloroform, hexane (<1.1)	66
	PMMA/graphene	$NO_2/10$	1.06	Hexane, ethanol, xylene (<1.02)	67
Others	PDQT	$NH_3/10$	30	H_2S, NO_2, SO_2 (<10)	68
	DPPBu-BT	$NH_3/10$	1.9	Ethanol, ethylene (<1.009)	69
	PEI/carbon black	Nonanal/1	0.01	Dodecane, ethanol, (<1.017)	70

Heterojunctions could introduce greater interfacial adsorption especially for mixed-dimensional composites with difficult conformal combination. For instance, Y. Qin et al.[72] prepared the core–shell stannous sulfide (SnS)/zeolitic imidazolate framework-8 (ZIF-8) heterostructure as a room-temperature methanol sensor. Tiny ZIF-8 nanocrystals were uniformly attached onto the surface of SnS nanosheets. During the synthesis process, S atoms on the SnS surface tightly attracted Zn ions, which not only induced the in situ growth of ZIF-8, but also promoted the formation of tight heterojunctions. Due to the difference in work function between SnS and ZIF-8, the hole accumulation layer (HAL) and electron accumulation layer (EAL) were generated at the interface, thus forming a heterogeneous junction. These heterojunctions amplified the conductivity variation after methanol exposure, and thus improved the selectivity. The selectivity factor for other interfering VOCs was $k = S_{gas}/S_{methanol}$. The k value of the interfering gases was much less than 1, indicating that the modification of ZIF-8 greatly improved the methane selectivity.

As a typical representative of heterojunctions composed of binary metal oxides, U. T. Nakate et al.[73] fabricated a novel gas sensor based on the composites of n-type ZnO nanorods and p-type NiO nanoplates. In order to further enhance the sensor performance, Pd NPs were introduced. The morphology of the ternary composites is shown in Fig. 8a. With respect to NiO/ZnO counterparts, the Pd NP-decorated NiO/ZnO sensors exhibited higher response and selectivity toward H_2 (Fig. 8b). The ternary sensor showed a gradient response with H_2 concentration at 225 °C (Fig. 8d). The relevant H_2-sensing mechanism is schematically illustrated in Fig. 8c. Upon close contact, an interfacial depletion region between NiO and ZnO was formed. When exposed to H_2, the H_2 molecules reacted with chemisorbed oxygen on the material surface and released electrons. These electrons consumed the holes which led to the increase of the sensor resistance. Meanwhile, with the increase of the potential barrier, the electrons migrated and the depletion region was extended, resulting in a further increase in resistance.

2D layered nanomaterials can also be functionalized by metal oxides such as SnO_2, ZnO and TiO_2 to construct heterojunctions. For example, the incorporation of TiO_2 quantum dots could convert p-type WS_2 nanosheets to an n-type one, simultaneously realizing a 17-fold larger response toward NH_3 with high selectivity.[74] It was reported that the

rGO/ZnO sensor showed higher conductivity and better detection selectivity to H_2 than the pure ZnO one.[75] H. Yan et al.[76] successfully synthesized the composites of SnO_2 nanoparticles and MoS_2 nanosheets by a two-step hydrothermal method. The $SnO_2@MoS_2$ sensor showed a high response to ethanol (Fig. 9c and d) and good selectivity (Fig. 9b). As shown in Fig. 9a, MoS_2 nanosheets with a high surface area served as a platform to attach SnO_2 nanoparticles which prevented their aggregation. This porous nanostructure provided numerous sorption sites and promoted the diffusion of ethanol molecules within the sensing layer. In addition, the activation energy was decreased.

Also, the heterojunction of 2D/2D layered materials is a popular alternative. N. M. Tran et al.[77] prepared a novel rGO/$Ti_3C_2T_x$ heterostructure to detect NO_2 gas (Fig. 10a). The morphological and structural analysis showed that MXene and rGO were hybridized well with sharp interfaces, accompanied with the increased specific surface area with regard to either single components (Fig. 10b and d). The obtained rGO/$Ti_3C_2T_x$ sensor showed higher response to NO_2 and better detection selectivity (Fig. 10c). The highly active surface terminal groups (–F, –OH, =O) of $Ti_3C_2T_x$ MXene nanosheets tended to capture O_2 molecules in synthetic air. Then partially adsorbed O_2 molecules were dissociated into O
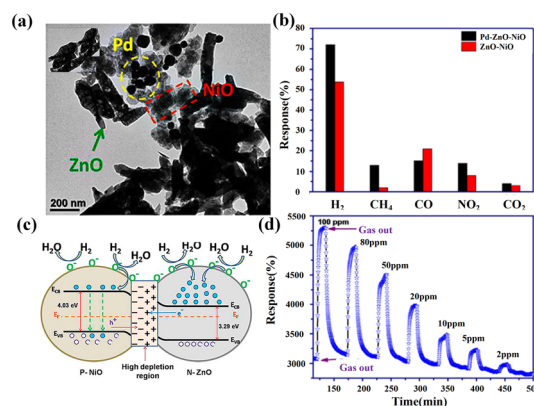

Fig. 8 (a) TEM image of the Pd/ZnO/NiO composites, (b) the selectivity of ZnO/NiO and Pd/ZnO/NiO sensors separately at 225 and 237 °C, (c) schematic H_2-sensing mechanism, and (d) dynamic resistance of the Pd/ZnO/NiO sensor as a function of H_2 concentration at 225 °C. Reprinted with permission from ref. 73 copyright 2019, Elsevier.
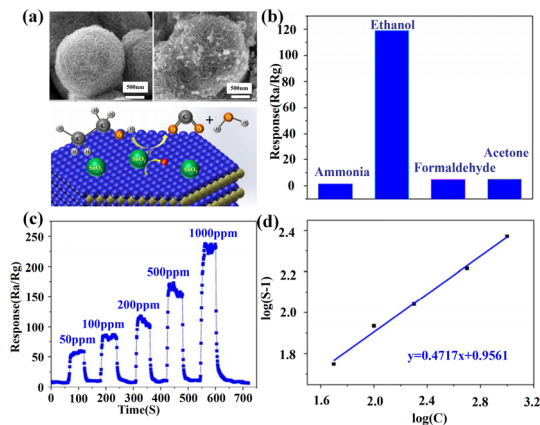
Fig. 9 (a) SEM image of pure MoS_2 and $SnO_2@MoS_2$ composites as well as the sensing mechanism for the composites, (b) selectivity, (c) dynamic response of the $SnO_2@MoS_2$ sensor as a function of ethanol concentration at 280 °C, and (d) dilogarithm fitting curve of the response–concentration relationship. Reprinted with permission from ref. 76 copyright 2015, The Royal Society of Chemistry.

atoms. Both O_2 molecules and O atoms probably extracted electrons from MXene *via* these terminal groups, resulting in the formation of oxygen ions (O^{2-} or O^-).[78,79] Due to the metallic nature of the $Ti_3C_2T_x$ material, the electron loss on its surface was not significant during this process. These active surface sites also promoted the adsorption of NO_2 molecules. Due to the higher electrophilicity, the physically-adsorbed NO_2 molecules were likely to acquire electrons from vicinal sites supplied by the rGO component, resulting in a remarkable increase in the density of majority carriers (holes). Moreover, the close contact between rGO and MXene allowed more electrons to be transferred to NO_2 molecules at a faster rate. Therefore, the heterojunctions increased the response and improved the selectivity.
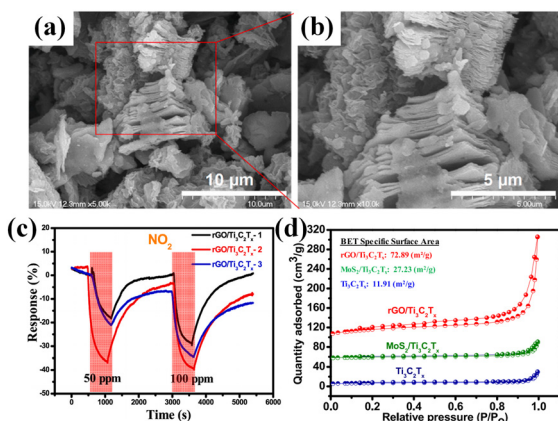
Fig. 10 (a) Schematic illustration of the NO_2-sensing mechanism of the $rGO/Ti_3C_2T_x$ heterostructure. (b) The nitrogen adsorption and desorption isotherms of $Ti_3C_2T_x$ MXene, $rGO/Ti_3C_2T_x$, and $MoS_2/Ti_3C_2T_x$ with BET surface areas. (c and d) $rGO/Ti_3C_2T_x$ heterostructure. Reprinted with permission from ref. 77 copyright 2019, The Royal Society of Chemistry.

2.2.2 Polymer modification. Polymers possessed a unique ability to provide a specific response, electron transfer, conformational change, and molecule-matched cavities, and thus played a critical role in the selectivity improvement.

In recent decades, conducting polymers such as polyaniline (PANI), poly(3,4-ethylenedioxythiophene):polystyrenesulfonate (PEDOT:PSS), and poly(3-hexylthiophene) (P3HT) have been extensively applied in this field.[64] The most well-studied example is PANI and its composite with a secondary material such as MOS, carbon nanotubes (CNT), and graphene-based derivatives. During the synthesis process of PANI, hydrochloric acid (HCl) could protonate PANI with N^+–H chemical bonds formed on the surface. The positive charge over nitrogen in PANI allowed a reversible interaction with NH_3 together with the products of neutral PANI and positive ammonium ion (NH_4^+). Therefore, PANI is often combined with other sensing materials to improve the NH_3 selectivity.[80] Y. Guo *et al.*[81] formed reduced graphene oxide (PPANI/rGO) by polymerizing aniline in a rGO solution. Next, the PANI nanoparticles (PPANI) and PANI nanofibers (FPANI) were successfully interlinked to produce the layered nanocomposite film (PPANI/rGO-FPANI) (Fig. 11c and d). The increased response of the composite to NH_3 (Fig. 11a and b) was mainly attributed to the synergistic effect and the high specific surface area. After adding PANI, NH_3 molecules could easily be adsorbed on PANI to provide electrons, thus increasing the resistance of PANI and further increasing the response (Fig. 11e). The lower electrical conductivity of PANI than that of rGO reduced the original resistance of the PPANI sensor. Moreover, PPANI strongly interacted with rGO through π–π interactions as an efficient
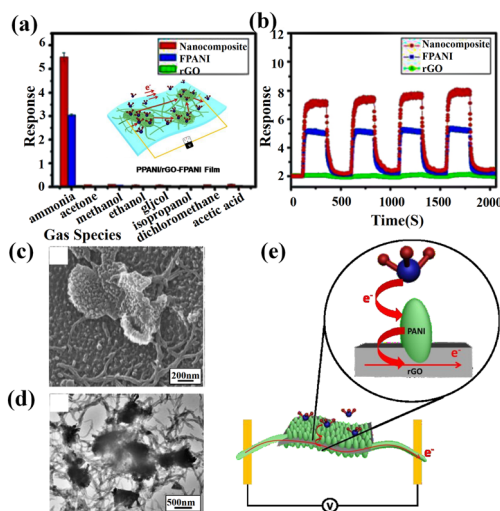
Fig. 11 (a) Gas sensing selectivity (averaged results with error bar) of the rGO film, FPANI and PPANI/rGO-FPANI nanocomposite film devices to various volatile gases. (b) The repeatability of the rGO, FPANI, and PPANI/rGO-FPANI nanocomposite film sensors (6 h sample) to 10 ppm NH_3. (c and d) SEM and TEM images of hierarchical PPANI/rGO-FPANI networks after polymerization. (e) Illustration of the NH_3-sensing mechanism in the PPANI/rGO-FPANI network. Reprinted with permission from ref. 81 copyright 2016, The Royal Society of Chemistry.

sensing channel to enhance the charge transfer. Thus, the selectivity of the composite to NH_3 gas was improved.

Molecular imprinting polymers (MIPs) are a class of cross-linked polymers that can bind target compounds with high specificity. Unlike ordinary polymers, the selectivity of MIPs depended not only on the solvation parameters of the gas molecules, but also on the shape and size of the template molecules. This allowed MIPs to distinguish target molecules from those with similar structures. Molecular imprinting techniques have been used to fabricate sensors with predetermined selectivity for gaseous molecules.[67] For example, T. Alizadeh et al.[66] successfully prepared a composite material of a nanoporous toluene-imprinted polymer, carbon powder, and n-eicosane. The MIP-based sensor exhibited a better toluene recognition than the non-imprinted polymer (NIP)-based counterpart (Fig. 12b). The interaction between the MIP and the analyte could be described by the following equation (eqn (1)):[82]

$$\text{Toluene} + \text{MIP} \underset{k_1}{\overset{k_2}{\rightleftharpoons}} \text{Toluene} - \text{MIP} \tag{1}$$
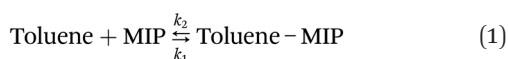
Herein, k_1 and k_2 represent the adsorption and desorption rate constants, respectively. According to eqn (1) and the diagram in Fig. 12a, when exposed to toluene vapor, the gas molecules diffused into the recognition cavity of the MIP. This caused the MIP between the adjacent conductive carbon black particles to swell, thereby distancing the conduction pathways and then increasing the sensor resistance. Since MIPs could be specifically designed, their selectivity could

also be significantly enhanced compared to NIPs. Fig. 12c shows the SEM image of the as-prepared MIP. Obviously, the MIP was a kind of highly porous material full of nanoscale pores, which provided a high surface area for molecular adsorption. Thus, the response to the target gas was enhanced and then the selectivity was optimized.

Recent developments enabled a surface modification of polymer film via different strategies to ameliorate the selectivity and sensing performance of gas sensors.[83] For instance, M. Castro et al.[84] developed a series of poly(1-caprolactone)-grafted carbon nanotubes (PCL-g-CNT) via the spaying-layer-by-layer strategy. According to the Henry Clustering (HC) model of the PCL-g-CNT conductive polymer composite (CPC) sensor,[85] at low concentrations ($0 < f < 0.5$) when only Henry diffusion occurred, solvent molecules could quickly enter the free volume of the amorphous phase at the scale of nanometer size, and finally changed the environment of CNT junctions through adsorption. For higher solvent concentrations ($f > 0.5$), the clustering of analytes led to a larger electrical signal due to swelling and important macromolecular conformational changes.[86] In this diffusion mode, the selectivity of CPC was not only driven by the matrix diffusion (analyte/polymer interaction) but also by the direct analyte adsorption on CNT (analyte/CNT interactions) and volume expansion. This leads to additional clustering reactions. Fitting parameters for chloroform using the HC model as depicted in eqn (2) are summarized in this study.[84] Among them, the fitting parameters for chloroform gas are: $f' = 0.001$, $n' = 3.75$, $k_H = 1.8$, $B = 4.26$. Compared to other cases, the HC model for chloroform required additional clustering factor $B = 4.25$ (for others gas, $B = 1$), so A_R for chloroform was 4 times larger than that for other gases, thus improving the selectivity.

$$A_R = k_H \times f + (f - f') \times (B \times f)^{n'} \tag{2}$$

where A_R is the sensor response, f is the solvent fraction (moles of solvent/moles of nitrogen) equal to gas concentration, f' is the solvent fraction over which clustering took place, k_H is Henry's diffusion parameter, n' represents the average number of solvent molecules per cluster, and B denotes the extra clustering factor.

Combining different materials to form heterojunctions is simple and widely studied, however, the selectivity is only improved to a limited extent. Due to the lack of accurate mechanisms to interpret the selectivity in polymer modification, the relevant discussion is usually treated with phenomenology. In addition, some limitations still exist such as high cost, high temperature sensitivity, low aging resistance, and poor storage stability.[87]

2.3 Specific target recognition

With respect to the previous two methods to improve the selectivity, specific target recognition does not alter the basic properties of sensitive materials such as energy levels, and is also relatively controllable. Moreover, this strategy introduces
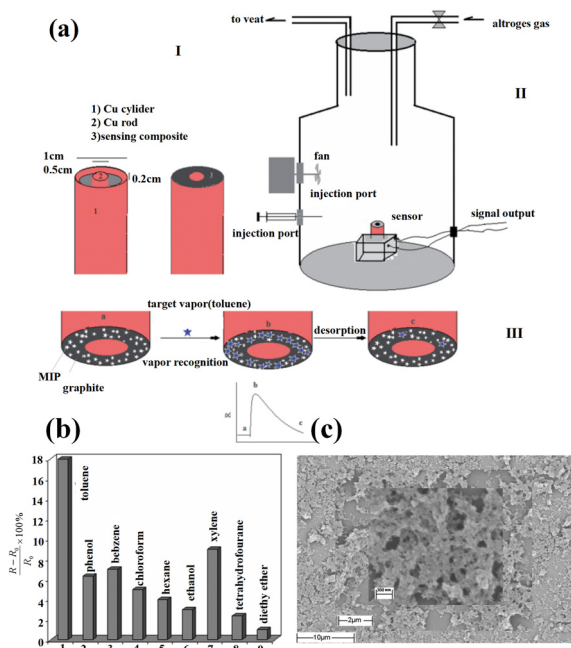
Fig. 12 (a) Schematic representation of the sensor device (I), vapor sampling system (II) and the relationship between the electrical signal and recognition mechanism (III), (b) response for different vapors (25 ppm), and (c) SEM image of the MIP. Reprinted with permission from ref. 66 copyright 2013, Taylor & Francis.

Table 4 Summary of specific object recognition methods

| Method	Sensor	Gas/Conc. (ppm)	Response	Selectivity coefficient	Ref.
Organometallic receptors	Carbon nanotube/polythiophene	DMMP/1%	1.15	Hexane, toluene ($<$1.03)	88
	Functionalized single walled carbon nanotubes	CO/200	1.01	CO_2,O_2 ($<$1.005)	89
	Carbon nanotube-based devices	Ethylene/50	1.8	Benzene, acetone, methanol ($<$1.05)	90
	Chemiresistive carbon nanotube sensors	NDMA/200	17	Hexane, water, acetone ($<$3)	91
Self-assembled monolayer	Organosilane SAMs at the surface of organic	Acetone/1%	2	—	92
	SAM-modified semiconductor nanowires	NO_2/0.4	2100	SO_2, NO, CO_2, NH_3, CO ($<$20)	93
	SAM of alkanedithiol	NO_2/100	16.02	CO, CH_3OH, H_2, NH_3 ($<$7)	94
	Densely packed SAM flexible sensor	Nitrobenzene/249	80	Methanol, n-hexane, toluene ($<$40)	95

NDMA: N-nitrosodimethylamine.

specific functional groups for target gases for selectivity optimization. Since some gases exhibit unique reactions with specific functional groups, we can incorporate these groups to match the key-to-lock interaction, and improve the chemical affinity between the material surface and the target molecules. In this regard, organometallic receptors and self-assembled monolayers (SAM) were usually employed. Table 4 summarizes some representative cases.[88–95]

2.3.1 Organometallic receptors. Organometallic complexes were inspired by enzyme or cell structure, such as haemoglobin-inspired CO receptors, and could be used for specific target recognition. B. Esser *et al.*[90] proposed a reversible chemical resin sensor capable of selectively detecting ethylene at the sub-ppm level. As shown in Fig. 13a, a mixture of single-walled carbon nanotubes (SWNTs) and a copper(I) complex based on a triazolyl (pyrazolyl) borate ligand were dropped between gold electrodes. During the fruit-ripening process, the combination of ethylene and the receptor ETR1 led to the translation of the ripening gene, and finally produced an enzyme that could induce the visualization of the ripening where cuprous iodide was found to be an important cofactor of the receptor ETR1.[96] Inspired by this principle, the copper(I) based complex was combined with CNTs to recognize ethylene gas. This was because the copper(I) base complex combined with ethylene to form complex 2, which reduced the interaction with the surface of CNTs, and increased the resistance of the SWNT network compared to the material without the decoration of the copper(I) base complex. Meanwhile, the response to other gases was unchanged. Thus, the selectivity to ethylene was promoted (Fig. 13b and c). In another report, M. He *et al.*[91] used cobalt(III) tetraphenyl porphyrin-functionalized SWCNTs to selectively detect *N*-nitrosodimethylamine (NDMA) in air. It was found that the modified SWCNTs possessed a superior performance compared to their direct blending mixtures. The response to NDMA was greater than 15 while less than 3 toward other interference gases, which indicated a good selectivity toward NDMA. In another study, a voltage-activated chemiresistive sensor consisting of iron porphyrins-functionalized single-walled carbon nanotubes (F-SWCNTs)

was reported.[97] It was well known that when CO was bound to the iron centres of hemoglobin, it competed with oxygen, and resulted in reduced blood oxygen levels and acute poisoning. The strong specific interactions between CO and iron porphyrins also produced a highly selective and customizable sensor. In particular, the sensor exhibited a significant increase of response toward CO when a negative gate voltage was applied.

2.3.2 Self-assembled monolayers. SAMs could produce different functional groups on a single surface. Recently,
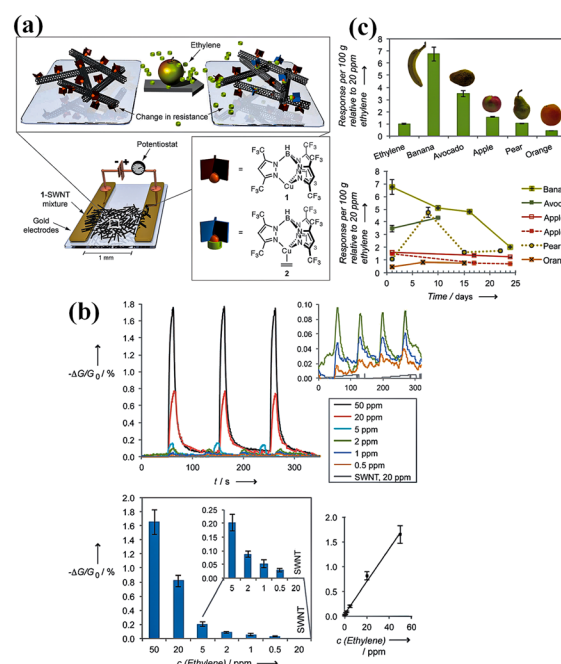
Fig. 13 (a) Ethylene detection by a chemiresistive sensor: the sensing mechanism of a mixture of SWNTs and copper complex 1, (b) sensor performance in terms of (1) response of SWNT devices to 0.5, 1, 2, 5, 20, and 50 ppm ethylene and of pristine SWNTs to 20 ppm ethylene, (2) average response and (3) the plot of average response *vs.* ethylene concentration. (c) Top: response of the 1-SWNT device to 100 g of different fruits and 20 ppm ethylene; bottom: response to fruit over several weeks. Reprinted with permission from ref. 90 copyright 2012, The Royal Society of Chemistry.
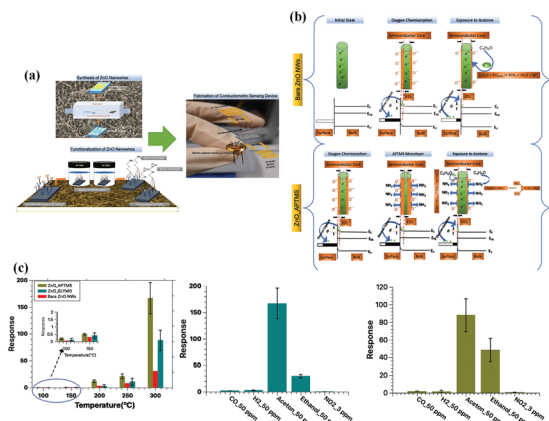
Fig. 14 (a) Synthesis of ZnO nanowires using the vapor–liquid–solid mechanism and the surface functionalization of ZnO nanowires with APTMS and GLYMO self-assembled monolayers, and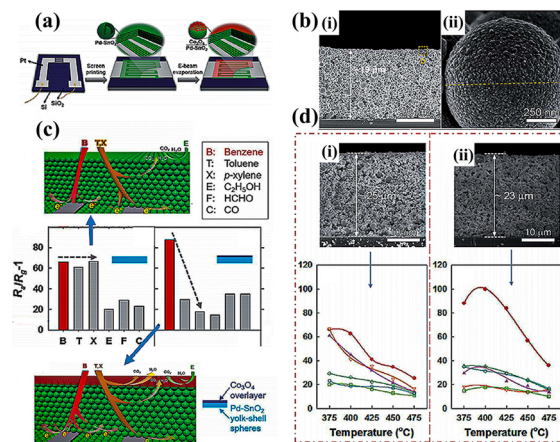 conductometric device, (b) the gas sensing mechanism of bare and SAM-functionalized ZnO NWs for acetone detection, (c) response *versus* temperature plot, and (d) the response of APTMS and GLYMO functionalized-ZnO nanowires toward 50 ppm acetone and other interfering gases at 300 °C. Reprinted with permission from ref. 99 copyright 2020, The Royal Society of Chemistry.

Fig. 15 (a) Schematic illustration of the sensor fabrication, (b) structural characterization of the Co_3O_4/Pd-SnO_2 composites, (c) the sensing performance and sensing mechanism of pristine and Co_3O_4-modified Pd-SnO_2 sensors, and (d) cross-sectional SEM images and gas-sensing characteristics of both sensors as a function of temperature. Reprinted with permission from ref. 132 copyright 2020, The Royal Society of Chemistry.

different types of silanes, such as (3-amino-propyl) trimethoxysilane (APTMS), 3-glycidoxypropyltrimethoxysilane (GLYMO), *N*-octadecyltrimethoxysilane (ODS), *etc.*, were used to create different functional surfaces to improve the sensor selectivity.[98] M. Singh *et al.*[99] functionalized ZnO surfaces with two different SAMs including APTMS and GLYMO for acetone detection. Fig. 14a schematically depicts the structure of pristine and SAM-functionalized ZnO nanowires. Obviously, the SAM-functionalized ZnO sensor possessed a higher response than the bare ZnO one (Fig. 14c). Compared to GLYMO functionalization, the APTMS case possessed a favorable acetone selectivity (Fig. 14d). Two aspects were responsible for this. On the one hand, when exposed to acetone, the electrons were released from reducing acetone molecules to the sensing material which reduced the resistance. On the other hand, within the APTMS-functionalized ZnO material, negatively-charged nucleophilic (–NH_2) groups of APTMS readily reacted with positively-charged carbon-heteroatom double bonds (C═O) in acetone molecules that acted as electrophilic centres, thus resulting in the formation of imine (($H_3C)_2$–C═N) and water molecule (Fig. 15b). Therefore, the gas–solid interactions enhanced the sensor response.

S. T. Marshall *et al.*[100] modified conventional Pd/Al_2O_3 catalysts with an *n*-alkanethiol SAM coating. The catalysts showed a selectivity to epoxybutane at 313 K of 11%, while the coated counterparts greatly improved the selectivity to up to 94%. Since the effect of surface sulfur simultaneously changes the geometric and electronic structures of platinum group metals, the varied crystallinity of the underlying surface reduces the activity of reactions that require multiple metal atoms and tightly-bound intermediates such as epoxide hydrogen. This is conducive to the bonding reaction with epoxybutane and thus the selectivity. In addition, the

n-alkanethiol SAM layer consisted of a sulfur atom "head" and a hydrocarbon "tail". And the precise control of the surface structure could be utilized to produce a clear near-surface environment, which boosted the adsorption energy of the epoxy.

At present, the method of specific target recognition still has the following problems. Firstly, specific functional groups can only distinguish between different classes of gases rather than the same class. For example, coporphyrin receptors possess a good affinity for amines and can be used to distinguish amines from other volatile organic compounds, but not various amines.[101] Secondly, not all gases can find unique functional groups to match with suitable sensitive materials.

2.4 Filters

Compared with specific target recognition, filters utilize other properties of the target analyte such as molecular size and surface affinity, which to some extent solves the problem of difficult matching between the target gas and functional groups.

Filters are one of the best ways to improve the selectivity of gas sensors, which was first demonstrated in the 1990s.[102] The filters were placed in front of the target sensor to control the composition of the gas mixture. There are two types of filter materials, one was prepared into a porous film that physically adsorbed gas molecules[103,104] and the other into a catalytic film that decompose gases. For example, CeO_2 could be utilized to separate oxygen at high temperatures,[105] while Pt and Pd films could permeate hydrogen. There are four basic configurations including a packed bed, a covering layer, a membrane and a separation column.[12] And Table 5 summarizes the work about filter-assisted gas sensors.[106–115]

Table 5 Summary filters combined with gas sensors

Filter Configuration	Filter material	Sensor	Gas/Conc. (ppm)	Response	Selectivity coefficient	Ref.
Packed bed	Carbon cloth	SnO_2	CO/15	1.25	Ethanol, ethyl, acetate, heptane ($\sim$0)	115
	Charcoal	Pd/In_2O_3	CH_4/500	11	Ethanol, methanol, acetone ($<$5)	107
	Zeolite 4A	Pd/SiO_2	CH_4/1000	60	CO, CO_2, VOCs ($<$15)	108
GC column	Porapak Q	SiO_2	Benzene/5	5	SO_2, CO ($<$2)	109
	Not specified	ZnO	Acetone/50	1.05	Acetone ($<$1.008)	110
Separation column	Activated alumina	Pt/SnO_2	Isoprene/0.5	7	Acetone, methanol, NH_3 ($<$5)	111
	Tenax TA	Pd/SnO_2	Methanol/5	20	Acetone, ethanol, H_2 ($<$10)	112
	Tenax TA	Pd/SnO_2	Formaldehyde/1	10	Acetaldehyde, acetone, CH_4 ($<$5)	113
Others	Indigo	Organic semiconductor	NO_2/0.1	4	Ozone ($>$0.5)	114

Adsorption filters harnessed the differences in polarity, hydrophilicity, boiling point, molecular weight, or size among multiple gas species to separate them. That is to say, the interference gases were adsorbed onto the filter while only allowing the target gas to pass through so as to enhance the selectivity of the downstream sensor. Recently, carbon-based filters,[116] mesoporous (2–50 nm) adsorbents such as silica gel,[117] porous polymers,[118] and activated alumina, as well as micropores ($<$2 nm) including membranes,[119] zeolites,[120,121] perovskites,[122,123] alumina,[124] and copper oxide[125] had been used for gas filtration. Recently, metal organic framework (MOF) materials, due to the high specific surface area, diverse structure and controllable porosity, have been developed to improve the selectivity of gas sensors.[126,127] For instance, T. Zhou *et al.*[128] synthesized two kinds of ZnO@zeolitic imidazolate framework (ZIF) core–shell structures with different pore sizes ($\sim$3.4 Å for ZIF-8, $\sim$4.8 Å for ZIF-71) to detect H_2, NH_3, ethanol, acetone, benzene and other gases. The ZnO@ZIF-8 structure showed a much higher selectivity for H_2 than that for ethanol and acetone, while the ZnO@ZIF-71 one exhibited an enhanced response to ethanol and acetone. The kinetic diameters of NH_3 (2.90 Å) and H_2 (2.89 Å) were respectively smaller than the pore sizes of ZIF-8 and ZIF-71, and could pass through the membranes easily. However, benzene molecules possessed a larger diameter (5.85 Å) than the pore size, thus leading to a negligible reaction. It could be concluded that the aperture of ZIFs determined the selectivity of ZnO@ZIF gas sensors. In addition, the BET data clearly unveiled that both ZnO@ZIF-8 and ZnO@ZIF-71 samples possessed a higher specific surface area and gas adsorption capacity than pure ZnO, which was also favorable for the improvement of selectivity.

As the gas-sensing measurement continued, the adsorption filter would be saturated with a deteriorated function. To overcome this issue, a catalytic filter was an effective alternative to enable a continuous measurement.[129] Catalytic filters could eliminate the effect of interfering gases by harnessing their differences in chemical reactivity. In this case, the interference gas was completely converted into an inert species to improve the sensor selectivity. Common catalytic filters included ceramic carriers (alumina, silica and ferric oxide) on precious metals (such as Pt, Pd and Au),[30] metal oxides,[130] mixed metal catalysts,[131] *etc.* Their surface composition, structure and operating temperature jointly determined the overall reactivity

and then the selectivity. For example, S.-Y. Jeong *et al.*[132] prepared a Pd-loaded micro-reactor sensing layer with a catalytic Co_3O_4 overlayer to improve the selectivity for benzene (Fig. 15a). Fig. 15b shows the SEM image of the cross section and the material surface. It could be found that the surface of Pd-loaded SnO_2 was covered by Co_3O_4. Then the performance of pristine and Co_3O_4-coated Pd-SnO_2 sensors was measured (Fig. 15d). Obviously, the Co_3O_4 coating significantly improved the selectivity because the interference gases including ethanol and formaldehyde were oxidized by the filter into inactive or less active species (CO_2 and H_2O). Benzene was efficiently transferred to areas close to the sensor electrode and converted into smaller and more active species, thus enhancing the sensing response.

In fact, these filters also exhibit adsorption saturation. In addition, most work focused on the modification considerations of individual sensors, which resulted in a relatively high regulation difficulty.

2.5 Electronic nose systems

Due to the limitations of single sensor regulation when improving the selectivity, electronic nose systems are currently widely used to perfect this situation. The electronic nose is a kind of olfactory bionic technology to simulate the working principle of animal nose. In general, the signal fingerprint of the gas sensor arrays within the electronic nose system was harnessed to classify different odors. For each gaseous sample, a set of signals were generated, which were then analyzed *via* pattern recognition strategies. An intact electronic nose system mainly included three parts: sensor array, information pre-processing and pattern recognition (Fig. 16). As the first successful attempt,[133] in 1982 three- and four-sensor arrays were used to simulate human olfaction.

2.5.1 Sensor arrays. As a common technology to improve the selectivity (Fig. 17),[134–137] a sensor array always employs different sensing layers, doping additives, preparation processes, device electrodes, and filter layers to obtain various sensor responses. When each gas sensor responded more selectively to specific chemical parameters or the molecular mass of the analyte, visualizing the "chemical" space was feasible. In this way, a small number of gas sensors (typically 3–32) could respond to a variety of different complex odors and allow the system to recognize an unknown odor.
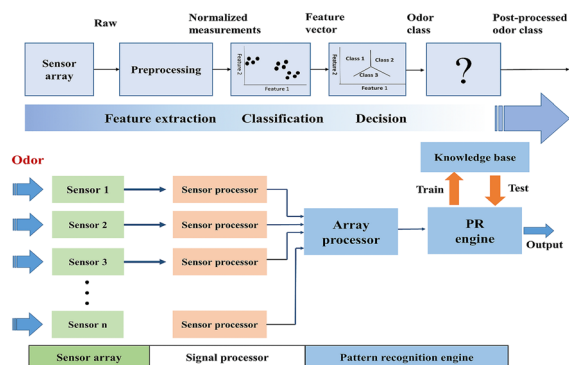
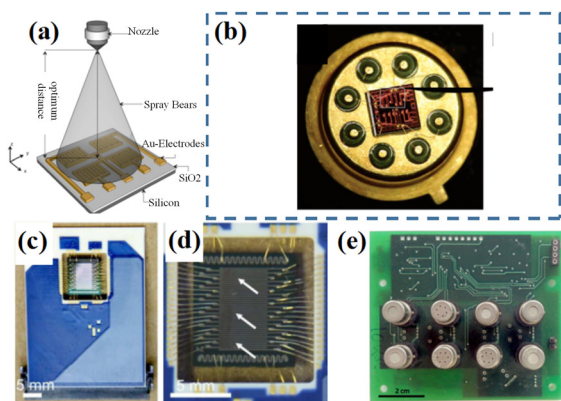**Fig. 16** Diagram illustrating the functioning of an electronic nose.

Fig. 17 (a) A schematic for the sensor array layout as well as the spray setup. Reprinted with permission from ref. 134 copyright 2015, Elsevier. (b) Simulated thermal plot of the designed 2 × 2 microheater array. Reprinted with permission from ref. 135 copyright 2006, American Chemical Society. (c and d) rGO-based multi-sensor array. Reprinted with permission from ref. 136 copyright 2013, The Royal Society of Chemistry. (e) Real image of a sensor array with different selective sensing layers. Reprinted with permission from ref. 137 copyright 2017, Elsevier.

responses. The data matrix was then processed with stoichiometric techniques so that unknown samples could be compared *via* this library. Common pattern recognition methods included artificial neural network (ANN)[139] and subspace projection such as principal component analysis (PCA),[140] linear discriminant analysis (LDA),[141] fast Fourier transform (FFT),[142] discrete wavelet transform (DWT),[143] *etc.* In addition, the curve fitting method,[144] waveform descriptor,[145] nonlinear subspace projection (self-organizing mapping, Sammons mapping, *etc.*), and clustering in feature space[146] were also employed in this field.
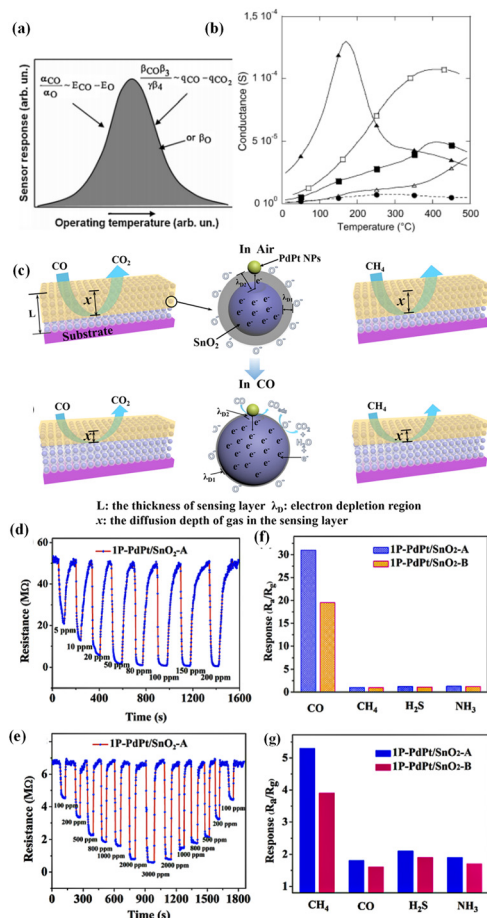
With the increasing requirements of algorithm accuracy, it was necessary to carry out the compensation treatment on the effect of temperature, baseline drift, humidity and so on for the data set. So many methods were used to pre-process the test data. For example, the machine learning algorithm (ML) was more suitable to eliminate the influence of the response fluctuation. Advanced methods for drift component correction (CC) contained PCA and partial least squares algorithm (PLS) from the first principal component of the data set.[147] This correction allowed the removal of highly correlated changes from one example to another. A generalization of this method was called component correction for common principal component analysis (CC-CPCA).[148] The drift of a sensor response could also be compensated for by periodic functions such as Fourier and wavelet transform.[148] Furthermore, V. V. Krivetskiy *et al.*[149] employed statistical signal shape analysis (SSA) to implement the response preprocessing of temperature-modulated MOS gas sensors, which enabled a lower effect of the response fluctuation and baseline drift and then an improved recognition ability of PCA, DWT, PCF and ML algorithms for closely related gases in realistic atmospheric conditions.

2.6 Others strategies

2.6.1 Temperature control. As is well known, the response of electronic-film gas sensors depended on the operating temperature.[150,151] With the initial temperature increase, more gas molecules possessed enough energy to overcome the activation barrier and participated in the sensing reaction, and thus boosted the sensor response.[152] When the response achieved a summit, the further increase of temperature adversely reduced the diffusion depth of the target gas within the sensing layer, which led to a lowered material utilization and then a decreased response.[153] The overall temperature–response relationship always presented a volcanic-shaped tendency (Fig. 18a). Due to the different activation energies required to be oxidized, each target gas exhibited its own optimal operating temperature (Fig. 18b), thus enabling the temperature control to tune the sensor selectivity.[151,154,155]

There were numerous reports utilizing this strategy to promote the selectivity. G. Li *et al.*[156] realized the dual selectivity of CO and CH_4 detection by using PdPt NPs with significant differences in the activation capacity of CO and

For example, A. Star *et al.*[135] modified SWNTs by site-selective electroplating of several catalytic metals (Pd, Pt, Rh, and Au) to prepare multiple sensors with different responses to analyte gases (H_2, CH_4, CO, and H_2S). An integrated sensor array based on rGO was also used to improve the selectivity,[136] with each sensor in the array possessing a unique response due to the irregular structure of the rGO film at the scale of nanosize. The resulting sensor system could reliably identify gases of nearly identical chemical properties. Also, the technology was equally applied for MOS gas sensors.[138] The diversity of MOS and their ability to measure at different temperatures were critical for predicting the concentration of individual gases in a mixture, overcoming the selectivity limitation on individual MOS sensors.

2.5.2 Pattern recognition. Each sensing material always exhibits its limitation on the detection selectivity. In this case, pattern recognition was a potential method to overcome this. When multiple gaseous samples were analyzed, a data matrix was generated that could form a "library" of known

Fig. 18 (a) Temperature-dependent response of MOS sensors toward CO, (b) temperature-dependent response of the SnO₂ sensor toward C₂H₅OH (50 ppm), H₂ (500 ppm), CO (300 ppm), and CH₄ (1000 ppm). Reprinted with permission from ref. 151 copyright 2005, Elsevier. (c) Schematic illustration of the CO-sensing mechanism of PdPt/SnO₂ at different working temperatures. The response of the obtained samples toward (d) 50 ppm CO and (e) 500 ppm CH₄ at different working temperatures, the response of the PdPt/SnO₂ sensors on successive exposure to 1000 ppm CH₄ and 50 ppm of other hazardous gases in the coal mine at (f) 100 °C and (g) 320 °C, respectively. Reprinted with permission from ref. 156 copyright 2019, American Chemical Society.

CH₄ at different temperatures of 100 and 320 °C. As shown in Fig. 18c–e, CO possessed a higher oxidation barrier at lower temperature to be activated by PdPt NPs, and then reacted with oxygen adsorbed on the MOS surface. However, the catalytic combustion of CH₄ usually required high temperature (over 350 °C) due to its non-polarity and strong stability (Fig. 18f and j). F. Xu et al.[157] investigated the response of ZnO toward four volatile organic compounds (ethanol, methanol, acetone and formaldehyde) at different temperatures from 20 to 400 °C, and analyzed the selectivity parameters. It was found that the stronger the broken bond, the higher the optimal temperature. In order to maximize the response, gas species with a larger molecular structure required higher temperature. Therefore, low temperature benefited the selectivity for small molecules with fewer and weaker bonds.

However, the approach discussed in the present section could not completely resolve the problem of low selectivity for MOS gas sensors because the temperature profiles of the sensing signals were too broad and there were too many gas species with similar temperature dependences.

2.6.2 Humidity-activated mechanism. The latest research has found that the humidity-activated sensing mechanism provides a new approach for highly selective detection of target gases.[158–160] For example, L. Liu et al.[158] developed an environmentally friendly and non-toxic biological NH₃ sensor with poly-L-aspartic acid (PAA) and L-glutamic acid (GA) as the sensing material. The results show that at room temperature, the response to 50 ppm NH₃ can reach 9.2 at 80% RH. This is because, under high humidity the water pre-adsorbed by the sensitive membrane attaches and dissolves NH₃ through the proton transfer reaction to produce NH₃⁺; moreover, the humidity-activated hydrogel can facilitate the formation of salt while the carboxyl group of GA reacts with NH₃ to form carboxylic acid, which is then ionized to ammonium radical and RCOO⁻ in the liquid phase.

In fact, humidity-activated sensing is a complex process that includes acid–base adsorption, ion-conduction formation, and reactions among various functional groups. In addition, the humidity activation mechanism can only be applied to specific conditions and sensitive materials, which needs more in-depth investigation.

2.6.3 Bias voltage modulation. Previous studies had verified that the modulation of bias voltage could optimize the selectivity of gas sensors.[161] This was because, the adsorption of various substances on the material surface was determined by the chemical potential of the adsorbed object. Thus, the electric potential, i.e., the bias pressure, was also a factor controlling the adsorption process. After the voltage was applied, the potential distribution along the material surface would be distorted. And the shape and size of this distortion depended on the target gas species, which was used to identify different gases.[162]

However, this technique was very limited. For example, in order to distort the potential distribution, the applied bias voltage must be high enough,[163] which was difficult to achieve. In addition, high bias voltage would induce the heating of the sensing film, causing the transient response to be remarkably different from the ideal situation.[164]

3. Summary and outlook

At present, how to improve the selectivity of gas sensors is a key challenge. In this review, the methods to achieve this goal are summarized. Firstly, we discussed two popular sensing mechanisms: the oxygen adsorption model and the charge transfer model. Subsequently, the methods to improve the selectivity were categorized including catalysis sensitization, composite construction, specific target recognition, filters, electronic nose systems, temperature/bias voltage control, and humidity modulation. For each method, examples were given to illustrate its concept and reveal its mechanism. Although each

strategy showcases some success, the existing limitations could not be ignored.

(I) For the single-element doping mentioned earlier, there may be drawbacks such as introducing unwanted impurity levels, agglomeration, and uncontrollability. In addition to bimetallic doping to overcome the limitations, researchers can further employ theoretical calculation to more accurately control the amount of doping.

(II) To address the issue of limited selectivity for heterojunctions, an emerging approach is to use hollow heterojunctions that combine hollow structures of two materials. The unique porous structure not only provides a large specific surface area and rich activity, but also enables short-distance charge carrier transport. For the drawbacks of polymer modifications, further research on their mechanisms is needed. For example, G. Becskereki et al.[165] had thoroughly analyzed the selectivity mechanism of imprinted polymers in batch adsorption, binding analysis, chromatography, solid phase extraction, sensors, membranes, and catalysts. In addition, the polymer modification also demonstrates some limitations such as high cost and poor storage stability.[87] Researchers can try various methods to eliminate these shortcomings such as adding hydrophobic clays, developing new active polymers, etc.

(III) As stressed above, organometallic receptors can only distinguish between different classes of gases rather than the same class. For example, ethylene receptors show high selectivity to ethylene under the interference of toluene, ethyl acetate, ethanol, chloroform and n-hexane gases, but similar reactions to acetonitrile, tetrahydrofuran and acetaldehyde. If the sensor is disturbed by these vapors of high concentration, a false positive reaction would occur.[166] To address this limitation, organic ligands could be incorporated into composites. For example, various metals (Co, Ni, Cu, Zn, Cr, and Mn) were incorporated with N-nitrosodimethylamine (NDMA).[91]

(IV) To improve the selectivity via SAMs, electron transfer must be realized between the target gas and the sensing layer through SAMs so as to obtain a detectable response. Therefore, apart from determining the optimal SAMs, we also need to compare the Fermi level of the core sensing material with the energy level of the SAM–target complex.

(V) Currently, the most used filters are passive membranes with different diffusion parameters, which depended on the adsorption affinity of gas molecules on the screen and the pore–molecule size relationship. If there is no expected gas reaction or desorption, such adsorbent filters may become saturated when exposed to the interfering gas of large concentration. The selective catalytic reaction in the filter membrane is expected to overcome these limitations by catalyzing the conversion of interfering substances into harmless molecules.

(VI) The electronic nose system is not only more accurate and objective than the human nose in some cases, but also can be used in many harsh environments. It also expresses many limitations. First, the electronic nose tends to lose sensitivity in the presence of water vapor, which complicates the signal at high humidity.[167] We can solve the problem by drying the target gas or using the algorithm to correct the humidity. Second, reproducibility is another common and important issue associated with electronic noses.[168] To compensate for the temperature effect, some electronic noses employ an automatic sampler system to control the temperature. In addition, absolute calibration is impossible for a single target gas with high concentration. Besides, it is unable to obtain quantitative data on differences in gas types (fragrances, spoilage levels). All these problems need to be improved in the future.

To control the working temperature of CGS, light irradiation and doping with conducting nanofillers can be leveraged. In particular, introducing impurity energy levels to reduce the band gap width, and reducing interface density of states and grain boundaries will improve the material conductivity and lower the working temperature.[169] In addition, the existing strategies for selectivity optimization mostly focus on the single-dimensional information of the unit sensor (i.e., the sensitivity toward target gas), which challenged the modulation flexibility. In the future, more parameters can be collectively considered, such as response polarity (i.e., resistance increase or decrease upon exposure to target gas), response speed, recovery degree, and temperature/humidity effects, so as to evaluate the selectivity from multiple-dimensional perspectives, which enables more accurate and stable data.

We reviewed a number of methods to greatly improve the performance parameters of gas sensors in this work. By expanding the application fields, the future CGS can certainly play a key role in the development of some burgeoning scenarios (e.g., Internet of Things) with unprecedented selectivity.

Conflicts of interest

There are no conflicts to declare.

Acknowledgements

Notes and references

1 A. Kumar, H. Kim and G. P. Hancke, *IEEE Sens. J.*, 2012, **13**, 1329–1339.

2 C. Di Natale, R. Paolesse, E. Martinelli and R. Capuano, *Anal. Chim. Acta*, 2014, **824**, 1–17.

3 A. Ponzoni, E. Comini, I. Concina, M. Ferroni, M. Falasconi, E. Gobbi, V. Sberveglieri and G. Sberveglieri, *Sensors*, 2012, **12**, 17023–17045.

4 T. Xu, Y. Wang, Z. Xiong, Y. Wang, Y. Zhou and X. Li, *Nano-Micro Lett.*, 2023, **15**, 6.

5 Y. Wang and Y. Wang, *SmartMat*, 2023, **4**, e1130.

6 J. Li, Y. Wang, H. Song, Y. Guo, S. Hu, H. Zheng, S. Zhang, X. Li, Q. Gao and C. Li, *Adv. Compos. Hybrid Mater.*, 2023, **6**, 83.

7 J. Li, Y. Wang, X. Li, Q. Gao and S. Zhang, *J. Alloys Compd.*, 2021, **881**, 160551.

8 Y.-X. Zhang and Y.-H. Wang, *RSC Adv.*, 2017, **7**, 45129–45144.

9 G. Korotcenkov and B. Cho, *Sens. Actuators, B*, 2013, **188**, 709–728.

10 J. Walker, P. Karnati, S. A. Akbar and P. A. Morris, *Sens. Actuators, B*, 2022, **355**, 131242.

11 J. M. Smulko, M. Trawka, C. G. Granqvist, R. Ionescu, F. Annanouch, E. Llobet and L. B. Kish, *Sens. Rev.*, 2015, **35**, 340–347.

12 J. van den Broek, I. C. Weber, A. T. Güntner and S. E. Pratsinis, *Mater. Horiz.*, 2021, **8**, 661–684.

13 H. Hashtroudi, I. D. Mackinnon and M. Shafiei, *J. Mater. Chem. C*, 2020, **8**, 13108–13126.

14 M. Wusiman and F. Taghipour, *Crit. Rev. Solid State Mater. Sci.*, 2022, **47**, 416–435.

15 N. Joshi, T. Hayasaka, Y. Liu, H. Liu, O. N. Oliveira and L. Lin, *Microchim. Acta*, 2018, **185**, 1–16.

16 X. Liu, T. Ma, N. Pinna and J. Zhang, *Adv. Funct. Mater.*, 2017, **27**, 1702168.

17 J. Zhang, X. Liu, G. Neri and N. Pinna, *Adv. Mater.*, 2016, **28**, 795–831.

18 P. Barik and M. Pradhan, *Analyst*, 2022, **147**, 1024–1054.

19 P. T. Moseley, *Meas. Sci. Technol.*, 2017, **28**, 082001.

20 H. Ji, W. Zeng and Y. Li, *Nanoscale*, 2019, **11**, 22664–22684.

21 M. Wang, T. Hou, Z. Shen, X. Zhao and H. Ji, *Sens. Actuators, B*, 2019, **292**, 171–179.

22 W. He, W. Lv and J. H. Dickerson, *Gas Transport in Solid Oxide Fuel Cells*, 2014, pp. 9–17.

23 P. Shankar and J. B. B. Rayappan, *Sci. Lett. J.*, 2015, **4**, 126.

24 Y. Li, Z. Li, C. Chi, H. Shan, L. Zheng and Z. Fang, *Adv. Sci.*, 2017, **4**, 1600430.

25 Y. J. Hong, J. W. Yoon, J. H. Lee and Y. C. Kang, *Chem. – Eur. J.*, 2014, **20**, 2737–2741.

26 A. Katoch, S.-W. Choi, H. W. Kim and S. S. Kim, *J. Hazard. Mater.*, 2015, **286**, 229–235.

27 J. Zhao, W. Wang, Y. Liu, J. Ma, X. Li, Y. Du and G. Lu, *Sens. Actuators, B*, 2011, **160**, 604–608.

28 S.-J. Ha, J.-H. Kang, D. H. Choi, S. K. Nam, E. Reichmanis and J. H. Moon, *ACS Photonics*, 2018, **5**, 3621–3627.

29 A. I. Uddin, D.-T. Phan and G.-S. Chung, *Sens. Actuators, B*, 2015, **207**, 362–369.

30 H.-J. Kim, J.-W. Yoon, K.-I. Choi, H. W. Jang, A. Umar and J.-H. Lee, *Nanoscale*, 2013, **5**, 7066–7073.

31 D.-T. Phan and G.-S. Chung, *Int. J. Hydrogen Energy*, 2014, **39**, 620–629.

32 S. Cui, S. Mao, Z. Wen, J. Chang, Y. Zhang and J. Chen, *Analyst*, 2013, **138**, 2877–2882.

33 L. Huang, Z. Wang, J. Zhang, J. Pu, Y. Lin, S. Xu, L. Shen, Q. Chen and W. Shi, *ACS Appl. Mater. Interfaces*, 2014, **6**, 7426–7433.

34 S.-Y. Cho, H.-J. Koh, H.-W. Yoo, J.-S. Kim and H.-T. Jung, *ACS Sens.*, 2017, **2**, 183–189.

35 B. Cho, J. Yoon, S. K. Lim, A. R. Kim, S.-Y. Choi, D.-H. Kim, K. H. Lee, B. H. Lee, H. C. Ko and M. G. Hahm, *Sensors*, 2015, **15**, 24903–24913.

36 S.-Y. Cho, H.-J. Koh, H.-W. Yoo and H.-T. Jung, *Chem. Mater.*, 2017, **29**, 7197–7205.

37 T. Lan, Y. Zhao, J. Deng, J. Zhang, L. Shi and D. Zhang, *Catal. Sci. Technol.*, 2020, **10**, 5792–5810.

38 H. Yan, P. Song, S. Zhang, J. Zhang, Z. Yang and Q. Wang, *Ceram. Int.*, 2016, **42**, 9327–9331.

39 D. Sarkar, X. Xie, J. Kang, H. Zhang, W. Liu, J. Navarrete, M. Moskovits and K. Banerjee, *Nano Lett.*, 2015, **15**, 2852–2862.

40 C. Kuru, C. Choi, A. Kargar, D. Choi, Y. J. Kim, C. H. Liu, S. Yavuz and S. Jin, *Adv. Sci.*, 2015, **2**, 1500004.

41 C. R. Jung, A. Kundu, S. W. Nam and H.-I. Lee, *Appl. Catal., A*, 2007, **331**, 112–120.

42 K. Jiang, T. Chen, J. Sun, H. Quan and T. Zhou, *Nanomaterials*, 2023, **13**, 668.

43 J. Huang, J. Li, Z. Zhang, J. Li, X. Cao, J. Tang, X. Li, Y. Geng, J. Wang and Y. Du, *Sens. Actuators, B*, 2022, **373**, 132664.

44 G. Li, Z. Cheng, Q. Xiang, L. Yan, X. Wang and J. Xu, *Sens. Actuators, B*, 2019, **283**, 590–601.

45 C. Cullis, T. Nevell and D. Trimm, *J. Chem. Soc., Faraday Trans. 1*, 1972, **68**, 1406–1412.

46 L. Wang, Y. Kang, Y. Wang, B. Zhu, S. Zhang, W. Huang and S. Wang, *Mater. Sci. Eng., C*, 2012, **32**, 2079–2085.

47 G. Cui, G. Zhang and G. Zou, *Sci. Rep.*, 2013, **3**, 1–8.

48 A. Chen, X. Huang, Z. Tong, S. Bai, R. Luo and C. C. Liu, *Sens. Actuators, B*, 2006, **115**, 316–321.

49 M. Ivanovskaya, D. Kotsikau, G. Faglia, P. Nelli and S. Irkaev, *Sens. Actuators, B*, 2003, **93**, 422–430.

50 G. Sun, H. Chen, Y. Li, Z. Chen, S. Zhang, G. Ma, T. Jia, J. Cao, H. Bala and X. Wang, *Sens. Actuators, B*, 2016, **233**, 180–192.

51 M. Arafat, A. Haseeb, S. Akbar and M. Z. Quadir, *Sens. Actuators, B*, 2017, **238**, 972–984.

52 F. Li, X. Gao, R. Wang, T. Zhang and G. Lu, *Sens. Actuators, B*, 2017, **248**, 812–819.

53 D. Barreca, E. Comini, A. P. Ferrucci, A. Gasparotto, C. Maccato, C. Maragno, G. Sberveglieri and E. Tondello, *Chem. Mater.*, 2007, **19**, 5642–5649.

54 W. Tang, J. Wang, P. Yao and X. Li, *Sens. Actuators, B*, 2014, **192**, 543–549.

55 J. Hu, C. Zou, Y. Su, M. Li, N. Hu, H. Ni, Z. Yang and Y. Zhang, *J. Mater. Chem. C*, 2017, **5**, 6862–6871.

56 A. Chen, R. Liu, X. Peng, Q. Chen and J. Wu, *ACS Appl. Mater. Interfaces*, 2017, **9**, 37191–37200.

57 J. Li, H. Zhao, Y. Wang, R. Zhang, C. Zou and Y. Zhou, *Anal. Chem.*, 2022, **94**, 16160–16170.

58 Y. Zhou, Z. Hu, H. Zhao, Y. Wang, J. Li and C. Zou, *Anal. Chim. Acta*, 2023, 340825.

59 H. Zhao, J. Li, Y. Wang, R. Zhang, C. Zou and Y. Zhou, *IEEE Sens. J.*, 2022, **23**, 1908–1916.

60 W. Guo, L. Huang, B. Zhao, X. Gao, Z. Fan, X. Liu, Y. He and J. Zhang, *Sens. Actuators, B*, 2021, **346**, 130524.

61 X. Wang, D. Gu, X. Li, S. Lin, S. Zhao, M. N. Rumyantseva and A. M. Gaskov, *Sens. Actuators, B*, 2019, **282**, 290–299.

62 T. He, W. Liu, T. Lv, M. Ma, Z. Liu, A. Vasiliev and X. Li, *Sens. Actuators, B*, 2021, **329**, 129275.

63 R. Mangu, S. Rajaputra and V. P. Singh, *Nanotechnology*, 2011, **22**, 215502.

64 R. Zhang, Y. Wang, J. Li, H. Zhao, Y. Wang and Y. Zhou, *Microchim. Acta*, 2022, **189**, 308.

65 S. Hou, J. Yu, X. Zhuang, D. Li, Y. Liu, Z. Gao, T. Sun, F. Wang and X. Yu, *ACS Appl. Mater. Interfaces*, 2019, **11**, 44521–44527.

66 T. Alizadeh and F. Rezaloo, *Int. J. Environ. Anal. Chem.*, 2013, **93**, 919–934.

67 T. Alizadeh and L. Hamedsoltani, *J. Environ. Chem. Eng.*, 2014, **2**, 1514–1526.

68 R. Song, X. Zhou, Z. Wang, L. Zhu, J. Lu, D. Xue, Z. Wang, L. Huang and L. Chi, *Org. Electron.*, 2021, **91**, 106083.

69 D. Khim, G. S. Ryu, W. T. Park, H. Kim, M. Lee and Y. Y. Noh, *Adv. Mater.*, 2016, **28**, 2752–2759.

70 A. Daneshkhah, S. Vij, A. P. Siegel and M. Agarwal, *Chem. Eng. J.*, 2020, **383**, 123104.

71 W. Tang and J. Wang, *Acta Phys.-Chim. Sin.*, 2016, **32**, 1087–1104.

72 Y. Qin, J. Xie, S. Liu and Y. Bai, *Sens. Actuators, B*, 2022, **368**, 132230.

73 U. T. Nakate, R. Ahmad, P. Patil, Y. Wang, K. S. Bhat, T. Mahmoudi, Y. Yu, E.-K. Suh and Y.-B. Hahn, *J. Alloys Compd.*, 2019, **797**, 456–464.

74 N. Huo, S. Yang, Z. Wei, S.-S. Li, J.-B. Xia and J. Li, *Sci. Rep.*, 2014, **4**, 5209.

75 V. Galstyan, E. Comini, I. Kholmanov, G. Faglia and G. Sberveglieri, *RSC Adv.*, 2016, **6**, 34225–34232.

76 H. Yan, P. Song, S. Zhang, Z. Yang and Q. Wang, *RSC Adv.*, 2015, **5**, 79593–79599.

77 N. M. Tran, Q. T. H. Ta and J.-S. Noh, *Mater. Chem. Phys.*, 2021, **273**, 125087.

78 Q. T. H. Ta, G. Namgung and J.-S. Noh, *Electron. Mater. Lett.*, 2019, **15**, 750–759.

79 X. Yang, H. Li, T. Li, Z. Li, W. Wu, C. Zhou, P. Sun, F. Liu, X. Yan and Y. Gao, *Sens. Actuators, B*, 2019, **282**, 339–346.

80 N. R. Tanguy, M. Thompson and N. Yan, *Sens. Actuators, B*, 2018, **257**, 1044–1064.

81 Y. Guo, T. Wang, F. Chen, X. Sun, X. Li, Z. Yu, P. Wan and X. Chen, *Nanoscale*, 2016, **8**, 12073–12080.

82 L. Feng, Y. Liu, X. Zhou and J. Hu, *J. Colloid Interface Sci.*, 2005, **284**, 378–382.

83 M. R. DashtArzhandi, A. Ismail, T. Matsuura, B. Ng and M. Abdullah, *Chem. Eng. J.*, 2015, **269**, 51–59.

84 M. Castro, J. Lu, S. Bruzaud, B. Kumar and J.-F. Feller, *Carbon*, 2009, **47**, 1930–1942.

85 A. Bouvree, J.-F. Feller, M. Castro, Y. Grohens and M. Rinaudo, *Sens. Actuators, B*, 2009, **138**, 138–147.

86 J. F. Feller, D. Langevin and S. Marais, *Synth. Met.*, 2004, **144**, 81–88.

87 C. Ouyang, S. Wang, Y. Zhang and Y. Zhang, *Polym. Degrad. Stab.*, 2006, **91**, 795–804.

88 F. Wang, H. Gu and T. M. Swager, *J. Am. Chem. Soc.*, 2008, **130**, 5392–5393.

89 S. Savagatrup, V. Schroeder, X. He, S. Lin, M. He, O. Yassine, K. N. Salama, X. X. Zhang and T. M. Swager, *Angew. Chem.*, 2017, **129**, 14254–14258.

90 B. Esser, J. M. Schnorr and T. M. Swager, *Angew. Chem., Int. Ed.*, 2012, **51**, 5752–5756.

91 M. He, R. G. Croy, J. M. Essigmann and T. M. Swager, *ACS Sens.*, 2019, **4**, 2819–2824.

92 M. Calhoun, J. Sanchez, D. Olaya, M. Gershenson and V. Podzorov, *Nat. Mater.*, 2008, **7**, 84–89.

93 M. W. Hoffmann, J. D. Prades, L. Mayrhofer, F. Hernandez-Ramirez, T. T. Järvi, M. Moseler, A. Waag and H. Shen, *Adv. Funct. Mater.*, 2014, **24**, 595–602.

94 S.-H. Hsiao, J.-X. Wu and H.-I. Chen, *Sens. Actuators, B*, 2020, **305**, 127269.

95 M. Li, H. Chen, S. Li, G. Wang, F. Wei, X. Guo and H. Tu, *Langmuir*, 2020, **36**, 1462–1466.

96 B. M. Binder, *Plant Sci.*, 2008, **175**, 8–17.

97 C. Paoletti, M. He, P. Salvo, B. Melai, N. Calisi, M. Mannini, B. Cortigiani, F. G. Bellagambi, T. M. Swager and F. Di Francesco, *RSC Adv.*, 2018, **8**, 5578–5585.

98 C. A. Schoenbaum, D. K. Schwartz and J. W. Medlin, *Acc. Chem. Res.*, 2014, **47**, 1438–1445.

99 M. Singh, N. Kaur, G. Drera, A. Casotto, L. Sangaletti and E. Comini, *Adv. Funct. Mater.*, 2020, **30**, 2003217.

100 S. T. Marshall, M. O'Brien, B. Oetter, A. Corpuz, R. M. Richards, D. K. Schwartz and J. W. Medlin, *Nat. Mater.*, 2010, **9**, 853–858.

101 S. F. Liu, A. R. Petty, G. T. Sazama and T. M. Swager, *Angew. Chem., Int. Ed.*, 2015, **54**, 6554–6557.

102 M. Fleischer, S. Kornely, T. Weh, J. Frank and H. Meixner, *Sens. Actuators, B*, 2000, **69**, 205–210.

103 D. J. Wales, J. Grand, V. P. Ting, R. D. Burke, K. J. Edler, C. R. Bowen, S. Mintova and A. D. Burrows, *Chem. Soc. Rev.*, 2015, **44**, 4290–4321.

104 M. Drobek, J.-H. Kim, M. Bechelany, C. Vallicari, A. Julbe and S. S. Kim, *ACS Appl. Mater. Interfaces*, 2016, **8**, 8323–8328.

105 H. Li, R. Wu, X. Tian, L. Han, T. Chen, B. Yang, Z. Zhi, Z. Hua and S. Fan, *Sens. Actuators, B*, 2023, **389**, 133872.

106 K. Nagashima and S. Suzuki, *Anal. Chim. Acta*, 1984, **162**, 153–159.

107 N. Lu, S. Fan, Y. Zhao, B. Yang, Z. Hua and Y. Wu, *Sens. Actuators, B*, 2021, **347**, 130603.

108 B. Yang, Z. Zhang, C. Tian, W. Yuan, Z. Hua, S. Fan, Y. Wu and X. Tian, *Sens. Actuators, B*, 2020, **321**, 128567.

109 J. Sun, Z. Geng, N. Xue, C. Liu and T. Ma, *Micromachines*, 2018, **9**, 408.

110 H. Jung, W. Cho, R. Yoo, H.-S. Lee, Y.-S. Choe, J. Y. Jeon and W. Lee, *Sens. Actuators, B*, 2018, **274**, 527–532.

111 J. van den Broek, A. T. Güntner and S. E. Pratsinis, *ACS Sens.*, 2018, **3**, 677–683.

112 J. van den Broek, S. Abegg, S. E. Pratsinis and A. T. Güntner, *Nat. Commun.*, 2019, **10**, 4220.

113 J. van den Broek, D. K. Cerrejon, S. E. Pratsinis and A. T. Güntner, *J. Hazard. Mater.*, 2020, **399**, 123052.

114 J. Brunet, L. Spinelle, A. Pauly, M. Dubois, K. Guerin, M. Bouvet, C. Varenne, B. Lauron and A. Hamwi, *Org. Electron.*, 2010, **11**, 1223–1229.

115 M. Schweizer-Berberich, S. Strathmann, W. Göpel, R. Sharma and A. Peyre-Lavigne, *Sens. Actuators, B*, 2000, **66**, 34–36.

116 X. Zhang, B. Gao, A. E. Creamer, C. Cao and Y. Li, *J. Hazard. Mater.*, 2017, **338**, 102–123.

117 A. A. Pesaran and A. F. Mills, *Int. J. Heat Mass Transfer*, 1987, **30**, 1037–1049.

118 K. Sakodynskii, L. Panina and N. Klinskaya, *Chromatographia*, 1974, **7**, 339–344.

119 P. Althainz, A. Dahlke, M. Frietsch-Klarhof, J. Goschnick and H. Ache, *Sens. Actuators, B*, 1995, **25**, 366–369.

120 M. Vilaseca, J. Coronas, A. Cirera, A. Cornet, J. Morante and J. Santamarıa, *Catal. Today*, 2003, **82**, 179–185.

121 G. Hagen, A. Dubbe, F. Rettig, A. Jerger, T. Birkhofer, R. Müller, C. Plog and R. Moos, *Sens. Actuators, B*, 2006, **119**, 441–448.

122 K.-Y. Lee, J.-C. Hsieh, C.-A. Chen, W.-L. Chen, H.-F. Meng, C.-J. Lu, S.-F. Horng and H.-W. Zan, *Sens. Actuators, B*, 2021, **326**, 128988.

123 Y. Zhuang, W. Yuan, L. Qian, S. Chen and G. Shi, *Phys. Chem. Chem. Phys.*, 2017, **19**, 12876–12881.

124 A. Ryzhikov, M. Labeau and A. Gaskov, *Sens. Actuators, B*, 2005, **109**, 91–96.

125 M. Frietsch, F. Zudock, J. Goschnick and M. Bruns, *Sens. Actuators, B*, 2000, **65**, 379–381.

126 J.-R. Li, R. J. Kuppler and H.-C. Zhou, *Chem. Soc. Rev.*, 2009, **38**, 1477–1504.

127 M. I. Nandasiri, S. R. Jambovane, B. P. McGrail, H. T. Schaef and S. K. Nune, *Coord. Chem. Rev.*, 2016, **311**, 38–52.

128 T. Zhou, Y. Sang, X. Wang, C. Wu, D. Zeng and C. Xie, *Sens. Actuators, B*, 2018, **258**, 1099–1106.

129 I. C. Weber and A. T. Güntner, *Sens. Actuators, B*, 2022, **356**, 131346.

130 M. Stoian, V. Rogé, L. Lazar, T. Maurer, J. C. Védrine, I.-C. Marcu and I. Fechete, *Catalysts*, 2021, **11**, 427.

131 D. Tayde and M. Lande, *Chem. Rev. Lett.*, 2021, **4**, 30–36.

132 S.-Y. Jeong, J.-W. Yoon, T.-H. Kim, H.-M. Jeong, C.-S. Lee, Y. Chan Kang and J.-H. Lee, *J. Mater. Chem. A*, 2017, **5**, 1446–1454.

133 K. Persaud and G. Dodd, *Nature*, 1982, **299**, 352–355.

134 A. Abdelhalim, M. Winkler, F. Loghin, C. Zeiser, P. Lugli and A. Abdellah, *Sens. Actuators, B*, 2015, **220**, 1288–1296.

135 A. Star, V. Joshi, S. Skarupo, D. Thomas and J.-C. P. Gabriel, *J. Phys. Chem. B*, 2006, **110**, 21014–21020.

136 A. Lipatov, A. Varezhnikov, P. Wilson, V. Sysoev, A. Kolmakov and A. Sinitskii, *Nanoscale*, 2013, **5**, 5426–5434.

137 A. Vergara, J. Fonollosa, J. Mahiques, M. Trincavelli, N. Rulkov and R. Huerta, *Sens. Actuators, B*, 2013, **185**, 462–477.

138 M. Leidinger, T. Sauerwald, W. Reimringer, G. Ventura and A. Schütze, *J. Sens. Sens. Syst.*, 2014, **3**, 253–263.

139 L. Trizio, M. Brattoli, G. De Gennaro, D. Suriano, R. Rossi, M. Alvisi, G. Cassano, V. Pfister and M. Penza, in *Sensors and Microsystems: AISEM 2011 Proceedings*, Springer, 2011, pp. 139–144.

140 M. Kermit and O. Tomic, *IEEE Sens. J.*, 2003, **3**, 218–228.

141 T. Itoh, Y. Koyama, Y. Sakumura, T. Akamatsu, A. Tsuruta, Y. Masuda and W. Shin, *Sens. Actuators, B*, 2023, **387**, 133803.

142 W. Sears, K. Colbow, R. Slamka and F. Consadori, *Sens. Actuators, B*, 1990, **2**, 283–289.

143 C. Distante, M. Leo and K. C. Persaud, *Discrete Wavelet Transforms, Biomed. Appl.*, 2011, p. 177.

144 J. Yan, F. Tian, Q. He, Y. Shen, S. Xu, J. Feng and K. Chaibou, *Sens. Mater.*, 2012, **24**, 57–73.

145 H. Liu, R. Wu, Q. Guo, Z. Hua and Y. Wu, *ACS Omega*, 2021, **6**, 30598–30606.

146 A. D. Wilson, *Procedia Technol.*, 2012, **1**, 453–463.

147 O. Tomic, T. Eklöv, K. Kvaal and J.-E. Haugen, *Anal. Chim. Acta*, 2004, **512**, 199–206.

148 N. J. Vickers, *Curr. Biol.*, 2017, **27**, R713–R715.

149 V. V. Krivetskiy, M. D. Andreev, A. O. Efitorov and A. M. Gaskov, *Sens. Actuators, B*, 2021, **329**, 129187.

150 N. Yamazoe and K. Shimanoe, *Sens. Actuators, B*, 2011, **154**, 277–282.

151 G. Tournier and C. Pijolat, *Sens. Actuators, B*, 2005, **106**, 553–562.

152 H.-B. Na, X.-F. Zhang, M. Zhang, Z.-P. Deng, X.-L. Cheng, L.-H. Huo and S. Gao, *Sens. Actuators, B*, 2019, **297**, 126816.

153 G. Sakai, N. Matsunaga, K. Shimanoe and N. Yamazoe, *Sens. Actuators, B*, 2001, **80**, 125–131.

154 T.-H. Kim, S.-Y. Jeong, Y. K. Moon and J.-H. Lee, *Sens. Actuators, B*, 2019, **301**, 127140.

155 S. Acharyya, S. Nag, S. Kimbahune, A. Ghose, A. Pal and P. K. Guha, *ACS Sens.*, 2021, **6**, 2218–2224.

156 G. Li, X. Wang, L. Yan, Y. Wang, Z. Zhang and J. Xu, *ACS Appl. Mater. Interfaces*, 2019, **11**, 26116–26126.

157 F. Xu, C. Zhou and H.-P. Ho, *J. Alloys Compd.*, 2021, **858**, 158294.

158 L. Liu, T. Fei, X. Guan, H. Zhao and T. Zhang, *Sens. Actuators, B*, 2021, **334**, 129625.

159 H. Zhao, L. Liu, X. Lin, J. Dai, S. Liu, T. Fei and T. Zhang, *ACS Sens.*, 2019, **5**, 346–352.

160 F. Pourfayaz, Y. Mortazavi, A. Khodadadi and S. Ajami, *Sens. Actuators, B*, 2008, **130**, 625–629.

161 A. Varpula, S. Novikov, A. Haarahiltunen and P. Kuivalainen, *Sens. Actuators, B*, 2011, **159**, 12–26.

162 M. Liess, *Sens. Actuators, B*, 2003, **95**, 46–50.

163 H. Tabata, Y. Sato, K. Oi, O. Kubo and M. Katayama, *ACS Appl. Mater. Interfaces*, 2018, **10**, 38387–38393.

164 T. Sauerwald, D. Skiera and C. D. Kohl, *Appl. Phys. A: Mater. Sci. Process.*, 2007, **87**, 525–529.

165 G. Becskereki, G. Horvai and B. Tóth, *Polymer*, 2021, **13**, 1781.

166 B. Esser, J. M. Schnorr and T. M. Swager, *Angew. Chem., Int. Ed.*, 2012, **51**, 5752–5756.

167 D. R. Wijaya, R. Sarno and E. Zulaika, *Data Brief*, 2018, **21**, 2414–2420.

168 W. Jia, G. Liang, Y. Wang and J. Wang, *Food Anal. Methods*, 2018, **11**, 2916–2924.

169 D.-H. Guan, X.-X. Wang, F. Li, L.-J. Zheng, M.-L. Li, H.-F. Wang and J.-J. Xu, *ACS Nano*, 2022, **16**, 12364–12376.

170 K. Hassan, A. I. Uddin and G.-S. Chung, *Sens. Actuators, B*, 2016, **234**, 435–445.

171 K. Y. Ko, J.-G. Song, Y. Kim, T. Choi, S. Shin, C. W. Lee, K. Lee, J. Koo, H. Lee and J. Kim, *ACS Nano*, 2016, **10**, 9287–9296.

172 C. Ouyang, Y. Chen, Z. Qin, D. Zeng, J. Zhang, H. Wang and C. Xie, *Appl. Surf. Sci.*, 2018, **455**, 45–52.